JOURNAL OF PROPULSION AND POWER
Vol. 17, No. 3, May–June 2001

Analysis of Heat-Driven Jet-Pumped Cooling System for Space Thermal Management

J. W. Nord,* W. E. Lear,† and S. A. Sherif‡
University of Florida, Gainesville, Florida 32611-6300

The solar integrated thermal management and power cycle is a new system that combines a thermal management cycle and a power producing cycle into a single self-contained unit. The system is powered entirely by solar thermal input via a concentrating solar collector. A jet pump provides the compression in the thermal management subsystem, reducing vibration and weight while increasing reliability. Other advantages of the system include constant temperature cooling, reduced number of system components, the ability to use a single working fluid, and the incorporation of a waste heat recovery unit. The methods used to analyze the jet pump and the overall system are described separately and in detail. Performance curves based on these analyses are then discussed.

Nomenclature

A	=	cross-sectional area, m^2
a	=	speed of sound, m/s
h	=	specific enthalpy, kJ/kg
M	=	Mach number
$\dot{m}$	=	mass flow rate, kg/s
P	=	pressure, MPa
$\dot{Q}$	=	heat transfer rate, kW
r	=	heat exchanger pressure ratio
s	=	specific entropy, kJ/kg · K
T	=	temperature, °C
V	=	velocity, m/s
$\dot{W}$	=	work rate, kW
η	=	efficiency, dimensionless
ρ	=	density, kg/m^3
σ	=	Stefan–Boltzmann constant, $5.67E-8$ W/m^{2}K^4
ϕ	=	entrainment ratio, $\dot{m}_s/\dot{m}_p$

Subscripts

de	=	diffuser exit
ei	=	evaporator inlet
evap	=	evaporator
me	=	mixing chamber exit
ne	=	primary nozzle exit
nt	=	primary nozzle throat
p	=	primary flow
pi	=	primary nozzle inlet
pe	=	pump exit
pump	=	mechanical pump
rad	=	radiator
re	=	radiator exit
s	=	secondary flow
sc	=	solar collector
se	=	secondary nozzle exit
si	=	secondary nozzle inlet
ss	=	state immediately downstream of shock
t	=	turbine
ti	=	turbine inlet
ts	=	isentropic turbine exit state

Received 8 February 2000; revision received 25 July 2000; accepted for publication 7 August 2000.

*Student, Department of Mechanical Engineering.
†Associate Professor, Department of Mechanical Engineering. Senior Member AIAA.
‡Associate Professor, Department of Mechanical Engineering, 237 MEB, P.O. Box 116300; sasherif@ufl.edu. Senior Member AIAA.

Introduction

TWO paramount issues in space operations are thermal management and power production. This paper analyzes a novel system for accomplishing both of these tasks. The solar integrated thermal management and power (SITMAP) cycle combines a thermal management subsystem and a power producing subsystem into a single modular unit. The system operates entirely on solar thermal input obtained via a concentrating solar collector. It uses this heat input to provide power and refrigeration and discards waste heat via a radiator. The system also provides for waste heat reclamation from other systems onboard the spacecraft, which directly reduces the heat input necessary from the solar collector.

The thermal management subsystem is essentially a vapor compression or refrigeration cycle, incorporating compression, condensation, expansion, and evaporation processes. There is a cooling load over an evaporator, and the waste heat of the entire system is rejected via condensation inside a radiator. One goal of the thermal management subsystem is to maximize the radiator temperature to take advantage of the relationship between radiation heat flux and radiator surface temperature. For a given heat rejection, the radiator size and weight vary inversely as the fourth power of the radiator surface temperature.

One feature of the SITMAP cycle is that a jet pump, rather than a compressor, provides the compression in the refrigeration subsystem. This is advantageous because a jet pump has no moving parts and, thus, increases reliability while decreasing vibration and weight. The jet pump acts as a common joining device for the two subsystems as it exchanges mass, momentum, and energy between the high-pressure, high-energy flow from the power subsystem and the low-pressure, low-energy flow from the refrigeration subsystem. This provides for a pressure increase in the refrigeration cycle.

Literature dealing with jet pumps is abundant and covers a wide array of applications. This includes the works of Bredikhin et al.,[1] Cunningham and Dopkin,[2] Cunningham,[3] Elger et al.,[4] Fabri and Paulon,[5] Fabri and Siestrunk,[6] Fairuzov and Bredikhin,[7] Holmes et al.,[8] Jiao et al.,[9] Lear et al.,[10] Marini et al.,[11] Neve,[12] and Sherif et al.[13] Other works involving thermally actuated cooling systems include those of Kakabaev and Davletov,[14] Chen,[15] Lansing and Chai,[16] and Chai and Lansing.[17] With the exception of the works of Fairuzov and Bredikhin,[7] Sherif et al.,[13] and Lear et al.,[10] which all dealt with two-phase flow in jet pumps, all of the other works mentioned were primarily focused on single-phase flows. The works of Fabri and Paulon[5] and Fabri and Siestrunk[6] discussed the possibility of choking the secondary flow in jet pumps under certain conditions. This type of choking in two-phase flow jet pumps is also discussed by Lear et al.[18]

The power subsystem drives the system and can be used to provide power for other onboard systems. It is essentially a Rankine cycle,

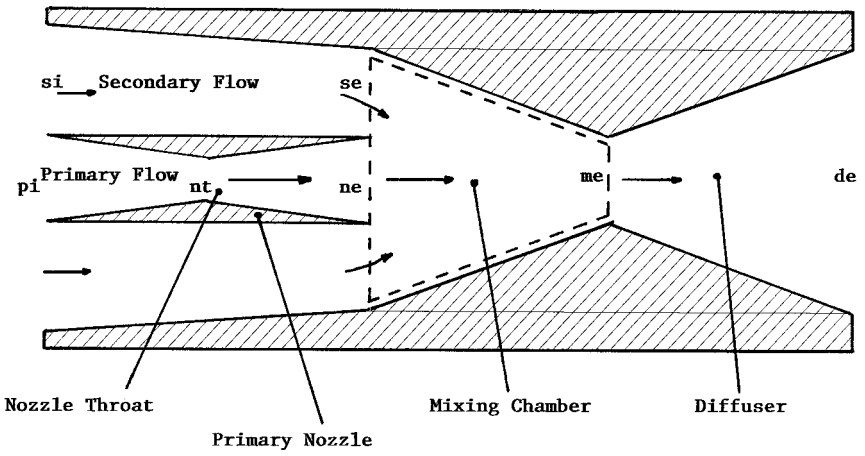

Fig. 1 Jet pump schematic; dashed lines define the control volume used for momentum analysis.

with, pump, boiler, turbine, and condenser. The turbine provides a mechanical work output that can be coupled to, among other things, the mechanical pump. This allows the system to be driven solely by solar thermal input. This paper considers the special case in which a work balance exists between the pump and turbine, though the system can be used to provide mechanical shaft work to other devices onboard the spacecraft. The flow leaving the turbine enters the jet pump to provide compression in the refrigeration subsystem as described earlier.

Analysis

The analysis described in this paper will be broken up into two parts. A general jet pump analysis that allows for two-phase flow will be discussed, followed by analysis of the SITMAP cycle given the results of the jet pump analysis.

Jet Pump

Figure 1 shows a schematic of the jet pump. The primary flow is expanded in a converging–diverging supersonic nozzle until the pressure matches that of the secondary exit. Constant pressure mixing takes place in the mixing chamber before entering the diffuser. The complete method for calculating the diffuser exit state and the jet pump geometry given the primary and secondary inlet states and the entrainment ratio ϕ is shown next.

Primary Nozzle

To obtain the properties at the nozzle throat, guess P_{nt} and use the assumption that $s_{nt} = s_{pi}$. Calculate the primary nozzle inlet velocity using the continuity equation

$$V_{pi} = [(\rho_{nt}/\rho_{pi})(A_{nt}/A_{pi})]V_{nt} \tag{1}$$

Calculate the velocity at the nozzle throat using conservation of energy

$$V_{nt} = \left\{(h_{pi} - h_{nt}) \Big/ \frac{1}{2}\left[1 - \left(\frac{\rho_{nt}}{\rho_{pi}}\frac{A_{nt}}{A_{pi}}\right)^2\right]\right\}^{\frac{1}{2}} \tag{2}$$

Calculate the Mach number at the nozzle throat using Eqs. (3) and (4). The s in Eq. (3) signifies an isentropic process,

$$a = \sqrt{\left(\frac{dP}{d\rho}\right)_s} \tag{3}$$

$$M = V/a \tag{4}$$

Iterate (change P_{nt}) until the Mach number is equal to unity.

To obtain the properties at the nozzle exit, assume that $s_{ne} = s_{nt}$ and that $P_{ne} = P_{se}$. For the current analysis, $P_{se}/P_{si} = 0.95$ was specified (this yields a velocity at the secondary exit of 45 m/s when state si is the stagnation state). Calculate the primary nozzle exit velocity using conservation of energy

$$V_{ne} = \left[2\left(h_{nt} + \tfrac{1}{2}V_{nt}^2 - h_{ne}\right)\right]^{\frac{1}{2}} \tag{5}$$

Calculate the ratio A_{nt}/A_{ne} using the continuity equation

$$A_{nt}/A_{ne} = (\rho_{ne}/\rho_{nt})(V_{ne}/V_{nt}) \tag{6}$$

Calculate the nozzle exit Mach number using Eqs. (3) and (4).

Secondary Flow

Specify A_{se}/A_{si} and guess A_{ne}/A_{se}. Estimate that $s_{se} = s_{si}$ and calculate the velocity at the secondary inlet using the continuity equation and the definition of entrainment ratio (note that P_{se} has been specified earlier):

$$V_{si} = \phi[(\rho_{ne}/\rho_{si})(A_{ne}/A_{se})(A_{se}/A_{si})]V_{ne} \tag{7}$$

Calculate the velocity at the secondary exit using conservation of energy and Eq. (7)

$$V_{se} = \left[2\left(h_{si} + \tfrac{1}{2}V_{si}^2 - h_{se}\right)\right]^{\frac{1}{2}} \tag{8}$$

Calculate the area ratio A_{ne}/A_{se} using the continuity equation and the definition of entrainment ratio

$$A_{ne}/A_{se} = (1/\phi)(\rho_{se}/\rho_{ne})(V_{se}/V_{ne}) \tag{9}$$

Calculate the Mach number at the secondary exit using Eqs. (3) and (4).

Mixing Chamber

Calculate the velocity at the mixing chamber exit using the continuity equation and the integral form of the momentum equation. The geometry of the mixing chamber is defined such that the mixing process occurs at constant pressure. Defining the control volume as shown in Fig. 1, the momentum equation [Eq. (10)] can be combined with Eq. (11) and the definition of entrainment ratio to obtain Eq. (12), the mixing chamber exit velocity

$$(P_{ne} - P_{se})A_{ne} = -\dot{m}_p V_{ne} - \phi\dot{m}_p V_{se} + (1+\phi)\dot{m}_p V_{me} \tag{10}$$

$$\dot{m}_p = \rho_{ne} A_{ne} V_{ne} \tag{11}$$

$$V_{me} = \frac{P_{ne} - P_{se} + \rho_{ne}V_{ne}^2[1 + \phi(V_{se}/V_{ne})]}{(1+\phi)\rho_{ne}V_{ne}} \tag{12}$$

Calculate the mixing chamber exit specific enthalpy and the area ratio A_{me}/A_{ne} using conservation of energy and the continuity equation, respectively,

$$h_{me} = [1/(1+\phi)]\left[h_{ne} + \tfrac{1}{2}V_{ne}^2 + \phi\left(h_{se} + \tfrac{1}{2}V_{se}^2\right)\right] - \tfrac{1}{2}V_{me}^2 \tag{13}$$

$$A_{me}/A_{ne} = (1+\phi)[(\rho_{ne}/\rho_{me})(V_{ne}/V_{me})] \tag{14}$$

Calculate the mixing chamber exit Mach number using Eqs. (3) and (4).

Diffuser

It is possible that the mixing chamber exit flow is supersonic. In such a case, a shock exists in the diffuser. This analysis assumes the shock occurs at the diffuser inlet where the Mach number is closest to unity and, thus, the stagnation pressure loss over the shock is minimized.

If $M_{me} > 1$, guess P_{ss} and assume Eqs. (15–18) apply for the shock

$$\rho_{me} V_{me} = \rho_{ss} V_{ss} \tag{15}$$

$$P_{me} + \rho_{me} V_{me}^2 = P_{ss} + \rho_{ss} V_{ss}^2 \tag{16}$$

$$h_{me} + \tfrac{1}{2} V_{me}^2 = h_{ss} + \tfrac{1}{2} V_{ss}^2 \tag{17}$$

$$\rho_{ss} = \rho(P_{ss}, h_{ss}) \tag{18}$$

Equations (15) and (16) can be combined to obtain the velocity downstream of the shock

$$V_{ss} = \frac{P_{me} + \rho_{me} V_{me}^2 - P_{ss}}{\rho_{me} V_{me}} \tag{19}$$

Equation (19) can be combined with Eq. (15) to obtain the density downstream of the shock. Equation (19) can also be used with Eq. (17) to obtain the specific enthalpy downstream of the shock, which can be used with Eq. (18) to obtain the density downstream of the shock. Iterate on P_{ss} until the density obtained from Eq. (15) matches that from Eq. (18). To obtain the diffuser exit state for the case of $M_{me} > 1$, follow the procedure for M_{me} less than or equal to 1, replacing the subscript me with ss.

If M_{me} is less than or equal to 1, then to obtain the properties at the diffuser exit, guess P_{de} and use the assumption that $s_{de} = s_{me}$. Calculate the velocity at the diffuser exit using the continuity equation

$$V_{de} = [(\rho_{me}/\rho_{de})(A_{me}/A_{ne})(A_{ne}/A_{de})]V_{me} \tag{20}$$

Calculate the velocity at the diffuser exit using conservation of energy

$$V_{de} = \left[2\left(h_{me} + \tfrac{1}{2} V_{me}^2 - h_{de}\right)\right]^{\frac{1}{2}} \tag{21}$$

Iterate (change P_{de}) until the continuity equation and conservation of energy yield the same diffuser exit velocity. Calculate the Mach number at the diffuser exit using Eqs. (3) and (4). The preceding jet pump analysis is general and applies to all flow regimes, including two-phase flow. The results can be used in the following SITMAP analysis.

SITMAP Cycle

Figure 2 shows the SITMAP cycle. The method used to achieve a converged solution for the SITMAP cycle given the jet pump inlet and exit states and entrainment ratio follows. The solar collector efficiency was estimated as 80%, and the pump, turbine, and radiator efficiencies were estimated as 95%. Frictional pressure losses in the system were lumped into an estimated pressure ratio over the various heat exchangers of $r = 0.97$. The jet pump primary inlet corresponds to the turbine exit state.

Overall Analysis

System convergence requires a double-iterative solution. The first step requires guessing the turbine inlet state (P_{ti} and T_{ti}). The specific enthalpy from Eq. (22) and that $P_{ts} = P_{pi}$ can then be used to calculate an isentropic turbine exit state. From the definition of turbine efficiency,

$$h_{ts} = h_{ti} - (h_{ti} - h_{pi})/\eta_t \tag{22}$$

Iterate on T_{ti} until the entropy corresponding to the current turbine inlet state matches that of the calculated isentropic turbine exit state.

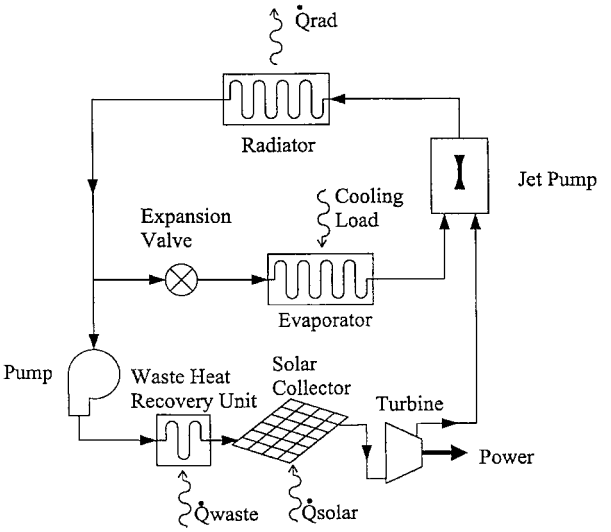

Fig. 2 Schematic of SITMAP cycle.

At this point, the correct inlet temperature corresponding to the guessed turbine inlet pressure and the specified turbine efficiency has been obtained. The next step is to invoke the work balance between the pump and turbine and use the heat exchanger pressure ratio to determine the validity of the guessed turbine inlet pressure

$$\dot{W}_t = \dot{m}_p(h_{ti} - h_{pi}) \tag{23}$$

$$\dot{W}_{pump} = \dot{m}_p/(\eta_{pump}\rho_{re})(P_{pe} - P_{re}) \tag{24}$$

$$P_{pe} = P_{re} + \dot{W}_{pump}\eta_{pump}\rho_{re}/\dot{m}_p \tag{25}$$

$$P_{ti} = P_{pe} r^2 \tag{26}$$

Iterate on P_{ti} (repeat the entire SITMAP analysis) until it matches that obtained by Eq. (26).

A converged solution has now been obtained for the SITMAP cycle. The following calculations complete the analysis:

$$h_{pe} = h_{re} + (h_{ti} - h_{pi}) \tag{27}$$

$$h_{ei} = h_{re} \tag{28}$$

$$\dot{Q}_{evap} = \phi\dot{m}_p(h_{si} - h_{ei}) \tag{29}$$

$$\dot{Q}_{rad} = \dot{m}_p(1 + \phi)(h_{de} - h_{re}) \tag{30}$$

$$\dot{Q}_{sc} = \dot{m}_p(h_{ti} - h_{pe}) \tag{31}$$

Note that Eq. (31) assumes the worst-case scenario of no waste heat recovery.

Solar Collector Model

The solar collector was modeled using a solar constant of $G_{sun} = 1353$ W/m^2. Equation (32) was used to estimate the area of the solar collector

$$A_{sc} = \dot{Q}_{sc}/(\eta_{sc} G_{sun}) \tag{32}$$

Radiator Model

Equation (33) represents the energy balance between the fluid and the radiator; emissivity has been lumped into an overall radiator efficiency, η_{rad},

$$dA_{rad} = -\dot{m}_p/(\eta_{rad}\sigma)T_{rad}^{-4}\, dh_{rad} \tag{33}$$

If superheat exists at the radiator inlet, Eq. (33) must be numerically integrated to account for decreasing temperature in the superheated region. For saturated flow, Eq. (33) can be readily integrated using the estimation of constant temperature at an average saturation pressure over the radiator.

A program called JetSit was developed to efficiently perform the preceding calculations and create performance graphs. JetSit's main

functions are to calculate the jet pump geometry and diffuser exit state and to use those results to calculate a solution to the SITMAP cycle. The program reads refrigerant properties from a data file, performs the necessary interpolations, uses the properties in the preceding analysis schemes, and writes the results to a file. Note that JetSit is able to analyze jet pump solutions for all flow regimes, including saturated flow.

Results and Discussion

This paper presents an analysis of a configuration of the SITMAP cycle in which there is a work balance between the pump and the turbine; that is, the turbine produces only enough mechanical work to drive the pump. In making performance curves, the following independent parameters are available: T_{si}, P_{si}, T_{pi}, P_{pi}, ϕ, and V_{se}. In all of the graphs shown, the secondary inlet corresponds to saturated vapor at 50°C. Graphs were also created for saturated vapor at 20 and 30°C, showing similar trends to those shown here. For all of the graphs, the velocity at the secondary exit is 45 m/s. A more detailed analysis of the jet pump that accounts for frictional losses should be performed in the future to determine the secondary exit velocity that provides for optimal jet pump performance. Refrigerant properties of R-134a were used in this analysis as reported by the American Society of Heating, Refrigerating, and Air Conditioning Engineers.[19]

Because this configuration is being considered for space applications, the primary goal is to minimize the weight per cooling load over the evaporator. At this early stage, we have chosen to consider as the figure of merit the radiator and solar collector areas per cooling load, assuming that the areas will be proportional to the weight. Therefore, system performance is considered optimized when the sum of the radiator and solar collector areas per cooling load (evaporator heat input) is minimized. Figures 3 and 4 show that for a given primary inlet pressure, performance increases as the primary inlet temperature decreases. This is because significant superheat at the primary inlet leads to significant superheat at the diffuser exit with little increase in diffuser exit pressure. Superheat at the radiator inlet serves no benefit; it simply adds to the radiator area. Figures 3 and 4 also show that for a given primary inlet temperature, the performance improves as the primary inlet pressure increases. This is because a higher primary inlet pressure leads to a higher diffuser exit (radiator inlet) pressure and, thus, a higher saturation temperature in the radiator. This increases the radiator heat flux, thereby reducing the radiator area.

For a given primary inlet pressure, the leftward extreme of the curve corresponds to saturated vapor at the primary inlet (turbine exit). This corresponds to the minimum temperature possible because liquid at the turbine exit is unacceptable. Therefore, Figs. 3 and 4 show that the optimum performance at a given pressure corresponds to saturated vapor at the primary inlet. Furthermore, performance improves as the primary inlet saturation temperature and pressure increase. This trend is repeated at various secondary inlet saturation temperatures and entrainment ratios. Figures 3 and 4 are representative of system performance holding the entrainment ratio constant. The following paragraphs discuss system performance as a function of the entrainment ratio.

Because it has been established that the optimal condition for a given entrainment ratio is saturated vapor at the primary inlet, it is relevant to investigate how the system performs as a function of the entrainment ratio for various saturated primary inlet temperatures. Figures 5 and 6 show that performance improves with entrainment ratio. This occurs in spite of increasing the entrainment ratio causing a decrease in the diffuser exit pressure and, thus, the saturation temperature (an effect that increases the radiator area for a given cooling load). The dominant effect is the increase in cooling load caused by the increase in mass flow rate in the refrigeration loop. The trend in the radiator area per cooling load (evaporator heat input) is strongly influenced by the relationship between radiator mass flow rate and evaporator mass flow rate because their ratio asymptotically approaches unity as entrainment ratio increases, $\dot{m}_{rad}/\dot{m}_{evap} = (1+\phi)/\phi$.

Figure 7 provides a closer look at radiator and solar collector areas as a function of entrainment ratio. The radiator area increases significantly with entrainment ratio due to the increase in mass flow rate in the refrigeration loop, but the solar collector area only changes slightly. The slight increase in solar collector area is due to the increased pump work necessary because the diffuser exit pressure decreases as the entrainment ratio increases. This explains why the solar collector area per cooling load decreases by a factor of

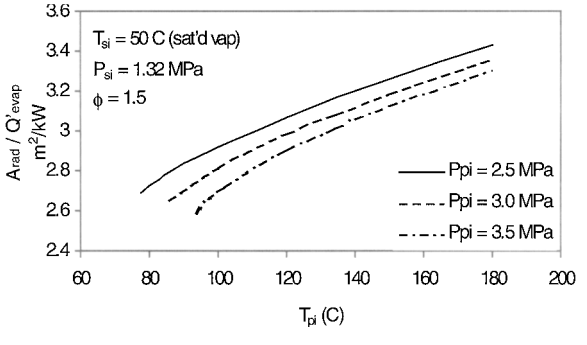

Fig. 3 Radiator area per cooling load as a function of primary inlet temperature.

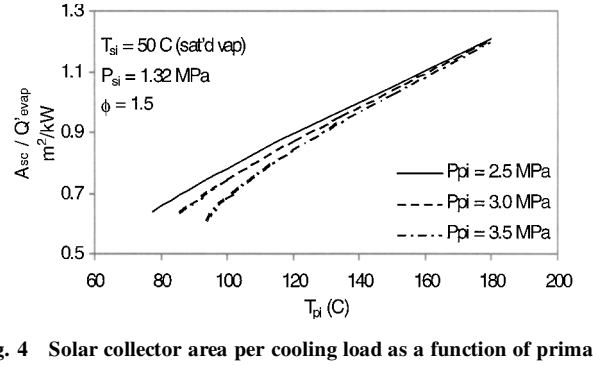

Fig. 4 Solar collector area per cooling load as a function of primary inlet temperature.

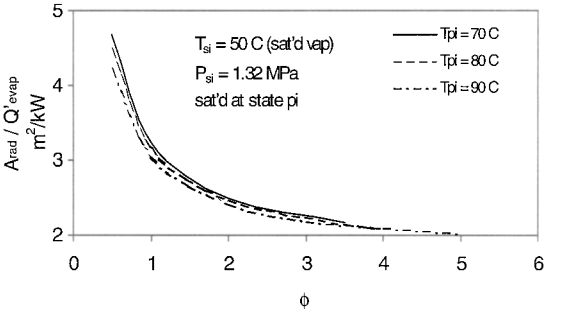

Fig. 5 Radiator area per cooling load as a function of entrainment ratio.

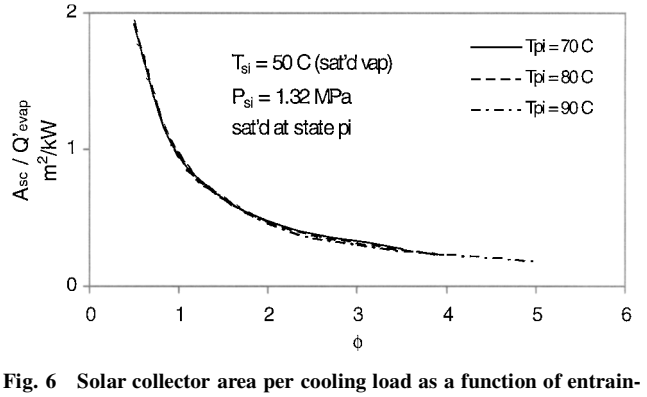

Fig. 6 Solar collector area per cooling load as a function of entrainment ratio.

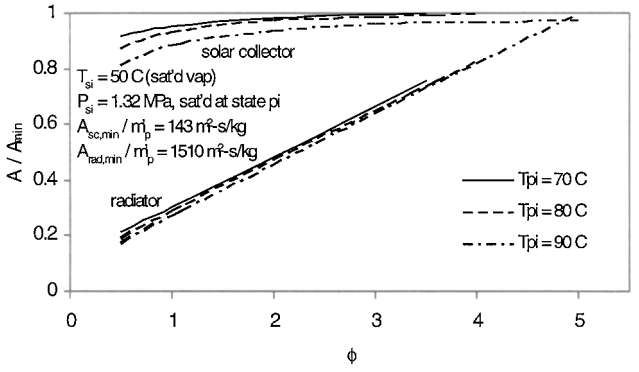

Fig. 7 Ratio of area to minimum area for the radiator and solar collector as function of entrainment ratio.

about 10, whereas the radiator area per cooling load decreases by a factor of about 3 (see Figs. 5 and 6). Although the radiator and solar collector areas increase with entrainment ratio, the cooling load increases such that the ratio of area per cooling load decreases for both devices.

At this point, it has been established that it is desirable to maximize the entrainment ratio while having saturated vapor at the primary inlet. However, as the entrainment ratio increases, the pressure rise over the jet pump in the refrigeration loop decreases. The entrainment ratio is, therefore, limited to a value corresponding to a pressure rise equal to the sum of the pressure losses over the radiator and the evaporator. In such a case, the vapor compression loop is simply a fluid circulation loop with essentially no refrigeration taking place. The rightward extremes of the curves in Figs. 5 and 6 approximately correspond to the maximum entrainment ratio for the respective primary inlet temperatures. Careful inspection reveals that the maximum entrainment ratio increases (and, thus, performance increases) with the primary inlet saturation temperature. With this, it can be concluded that the optimal case is the one with saturated vapor at the primary inlet and the maximum primary inlet temperature. The critical point of the working fluid is now what limits system performance (the critical point for R-134a occurs at 101.03°C).

It should be reiterated that these results apply to a specific configuration over a finite range of primary and secondary inlet temperatures and pressures. No excess turbine work was produced, and no waste heat recovery was utilized. Various configurations and ranges to be studied in the future could yield different results.

Conclusions

The following conclusions were drawn regarding performance in terms of combined radiator and solar collector areas per cooling load based on this study:

1) Performance improves as the primary inlet temperature approaches the saturation point for a given primary inlet pressure.

2) Performance improves as the primary inlet pressure increases for saturated vapor conditions at the primary inlet.

3) Performance is enhanced as the entrainment ratio increases.

4) For saturated vapor at the primary inlet, as the temperature increases, the maximum entrainment ratio increases, thus improving performance.

5) The critical point of the working fluid limits the entrainment ratio, thus limiting performance.

It follows from the preceding conclusions that, for the configuration and ranges studied, the system is most efficient when the entrainment ratio is so high that the vapor compression loop is simply a fluid circulation loop with essentially no refrigeration taking place. Note, however, that results might differ for different configurations and ranges of primary and secondary pressures and temperatures.

Acknowledgments

The authors are indebted to the financial support provided by the Thermal and Life Support Division of the NASA Marshall Space Flight Center. This work is partially based on a NASA/American Society for Engineering Education (ASEE) Summer Faculty Fellowship awarded to the third author in 1996 and 1997 under Grants NASA-MSFC-NGT8-52819 and NASA-MSFC-NGT8-52836, respectively. Support from the Department of Mechanical Engineering at the University of Florida is also gratefully acknowledged. The authors are also indebted to Patrick L. Hunt, Jon B. Holladay, Jim Owen, Bill Patterson, and Larry Turner of NASA Marshall Space Flight Center and NASA/ASEE program codirectors, G. R. Karr and L. M. Freeman.

References

[1]Bredikhin, V. V., Gorbenko, G. A., Nikonov, A. A., and Fairuzov, Y. V., "Mathematical Modeling of Thermo-Circulating Loops with Jet Pumps," *Hydrodynamic Processes in Multi-Phase Working Fluid Energy Plants*, Kharkov Aviation Inst., Kharkov, Ukraine, 1990, pp. 3–10 (in Russian).

[2]Cunningham, R. G., and Dopkin, R. J., "Jet Breakup and the Mixing Throat Lengths for the Liquid Jet Pump," *Journal of Fluids Engineering*, Vol. 96, No. 3, 1974, pp. 216–226.

[3]Cunningham, R. G., "Liquid Jet Pumps for Two-Phase Flows," *Journal of Fluids Engineering*, Vol. 117, No. 2, 1995, pp. 309–316.

[4]Elger, D. F., McLam, E. T., and Taylor, S. J., "A New Way to Represent Jet Pump Performance," *Journal of Fluids Engineering*, Vol. 113, No. 3, 1991, pp. 439–444.

[5]Fabri, J., and Paulon, J., "Theory and Experiments on Air-to-Air Supersonic Ejectors," NACA-TM-1410, Sept. 1958.

[6]Fabri, J., and Siestrunk, R., "Supersonic Air Ejectors," *Advances in Applied Mechanics*, Vol. 5, edited by H. L. Dryden and Th. von Karman, Academic Press, New York, 1958, pp. 1–33.

[7]Fairuzov, Y. V., and Bredikhin, V. V., "Two-Phase Cooling System with a Jet Pump for Spacecraft," *Journal of Thermophysics and Heat Transfer*, Vol. 9, No. 2, 1995, pp. 285–291.

[8]Holmes, H. R., Geopp, J., and Hewitt, H. W., "Development of the Lockheed Pumped Two Phase Thermal Bus," AIAA Paper 87-1626, June 1987.

[9]Jiao, B., Blais, R. N., and Schmidt, Z., "Efficiency and Pressure Recovery in Hydraulic Jet Pumping of Two-Phase Gas/Liquid Mixtures," *SPE Production Engineering*, Vol. 5, No. 4, 1990, pp. 361–364.

[10]Lear, W. E., Sherif, S. A., Steadham, J. M., Hunt, P. L., and Holladay, J. B., "Design Considerations of Jet Pumps with Supersonic Two-Phase Flow and Shocks," AIAA Paper 99-0461, Jan. 1999.

[11]Marini, M., Massardo, A., Satta, A., and Geraci, M., "Low Area Ratio Aircraft Fuel Jet-Pump Performance with and Without Cavitation," *Journal of Fluids Engineering*, Vol. 114, No. 4, 1992, pp. 626–631.

[12]Neve, R. S., "Diffuser Performance in Two-Phase Jet Pump," *International Journal of Multiphase Flow*, Vol. 17, No. 2, 1991, pp. 267–272.

[13]Sherif, S. A., Lear, W. E., Steadham, J. M., Hunt, P. L., and Holladay, J. B., "Analysis and Modeling of a Two-Phase Jet Pump of a Thermal Management System for Aerospace Applications," *International Journal of Mechanical Sciences*, Vol. 42, No. 2, 2000, pp. 185–198.

[14]Kakabaev, A., and Davletov, A., "A Freon Ejector Solar Cooler," *Geliotekhnika*, Vol. 2, No. 5, 1966, pp. 42–48.

[15]Chen, L.-T., "Solar Powered Vapor-Compressive Refrigeration System Using Ejectors as the Thermal Compressors," *Proceedings of the National Science Council*, No. 10, Pt. 3, May 1977, pp. 115–132.

[16]Lansing, F. L., and Chai, V. W., "A Thermodynamic Analysis of a Solar-Powered Jet Refrigeration System," Deep Space Network Progress Rept. 42-41, Jet Propulsion Lab., Pasadena, CA, Oct. 1977, pp. 209–217.

[17]Chai, V. W., and Lansing, F. L., "Performance of Solar-Powered Vapor-Jet Refrigeration Systems with Selected Working Fluids," Deep Space Network Progress Rept. 42-44, Jet Propulsion Lab., Pasadena, CA, Jan.–Feb. 1978, pp. 245–251.

[18]Lear, W. E., Sherif, S. A., and Parker, G. M., "Effect of Fabri Choking on the Performance of Two-Phase Jet Pumps," AIAA Paper 2000-3012, July 2000.

[19]ASHRAE, *1997 Fundamentals*, The American Society of Heating, Refrigerating, and Air-Conditioning Engineers, Inc., Atlanta, GA, 1997, pp. 19.24–19.27.